CORA Cork Open Research Archive
Cartlann Taighde Oscailte Chorcaí

Title	Chemically modified electrodes for recessed microelectrode array
Authors	Mohd Said, Nur Azura;Ogurtsov, Vladimir I.;Twomey, Karen;Nagle, Lorraine C.;Herzog, G.
Publication date	2016
Original Citation	Mohd Said, N. A., Ogurtsov, V. I., Twomey, K., Nagle, L. C. and Herzog, G. (2016) 'Chemically modified electrodes for recessed microelectrode array', Procedia Chemistry, 20, pp. 12-24. DOI: 10.1016/j.proche.2016.07.002
Type of publication	Article (peer-reviewed)
Link to publisher's version	http://www.sciencedirect.com/science/article/pii/S1876619616300109 - 10.1016/j.proche.2016.07.002
Rights	© 2016 The Authors. Published by Elsevier B.V. This is an open access article under the CC BY-NC-ND license https://creativecommons.org/licenses/by-nc-nd/4.0/ - https://creativecommons.org/licenses/by-nc-nd/4.0/
Download date	2026-11-01 22:06:47
Item downloaded from	https://hdl.handle.net/10468/6454



University College Cork, Ireland
Coláiste na hOllscoile Corcaigh

Available online at www.sciencedirect.com

ScienceDirect

Procedia Chemistry 20 (2016) 12 – 24

Procedia Chemistry

11th Asian Conference on Chemical Sensors, ACCS 2015

Chemically Modified Electrodes for Recessed Microelectrode Array

N.A. Mohd Said[a,b*], V.I. Ogurtsov[a], K. Twomey[a], L.C. Nagle[a] and G. Herzog[c]

[a]*Tyndall National Institute, University College Cork, Lee Maltings Prospect Row, Cork, Republic of Ireland*
[b]*Current affiliation: Biotechnology Research Centre, Malaysian Agricultural Research and Development Institute (MARDI), P.O Box 12301, General Post Office, 50774 Kuala Lumpur, Malaysia*
[c]*LCPME, UMR 7564, CNRS-Université de Lorraine, 405, Rue de Vandœuvre, 54600, Villers-lès-Nancy, France*

Abstract

Chemical modifications on recessed microelectrode array, achieved via electrodeposition techniques are reported here. Silicon-based gold microelectrode arrays of 10 µm microband and microdisc array were selected and functionalised using sol-gel and nanoporous gold (NPG) respectively. For electrochemically assisted self-assembly (EASA) formation of sol-gel, electrode surface was first pre-treated with a self-assembled partial monolayer of mercaptopropyltrimethoxysilane (MPTMS) before transferring it into the sol containing cetyltrimethyl ammonium bromide (CTAB)/tetraethoxysilane (TEOS):MPTMS (90:10) precursors. A cathodic potential is then applied. It was found that larger current densities were required in ensuring successful film deposition when moving from macro- to micro- dimensions. For NPG modification, a chemical etching process called dealloying was employed. NPG of three different thicknesses have been successfully deposited. All the modified and functionalized microelectrode arrays were characterized by both optical (SEM) and electrochemical analysis (cyclic voltammetry and impedance spectroscopy). An increase in surface area and roughness has been observed and such will benefit for future sensing application.

© 2016 The Authors. Published by Elsevier B.V. This is an open access article under the CC BY-NC-ND license (http://creativecommons.org/licenses/by-nc-nd/4.0/).
Peer-review under responsibility of Universiti Malaysia Perlis

Keywords: Electrochemically assisted self-assembly; Mesoporous silica films; Nanoporous gold; Recessed microelectrode array; Electrochemical impedance spectroscopy

* Corresponding author. Tel.: +6-03-8953-6095; fax: +6-03-8953-6154.
E-mail address: *nazurams@mardi.gov.my*

1876-6196 © 2016 The Authors. Published by Elsevier B.V. This is an open access article under the CC BY-NC-ND license (http://creativecommons.org/licenses/by-nc-nd/4.0/).
Peer-review under responsibility of Universiti Malaysia Perlis
doi:10.1016/j.proche.2016.07.002

1. Introduction

Micro- and nanoelectrode arrays offer a number of advantages for the electrochemical detection of analytes: (i) an improved mass transport leading to an increased sensitivity and better limits of detection; (ii) improved signal to noise ratio; (iii) reduced ohmic drop [1]. Using tools originally developed for the silicon integrated circuit (IC) industry, researchers are now fabricating miniaturized transducers from silicon and other materials [2] to be used in various biosensor applications such as environmental monitoring [3,4], food safety [5] and medical diagnostics [6]. These technologies allowed the fabrication of microelectrode arrays of different geometries and materials [7].

The surface of microelectrodes can be modified to achieve a desired selectivity or improve the sensitivity. Microelectrodes can be modified by electropolymerisation [8], to form a layer on the electrode surface sensitive to pesticides [9,10] or drugs [11]. Thiols can be spontaneously adsorbed onto gold nanoparticles immobilised on a gold microband array for the detection of organics in water [12,13] or they can be used as an anchor for the immobilisation of aptamers [14] and bacteriophage [15]. Antibodies for the amperometric detection of Aflatoxin M1 in milk could be immobilised via silanisation [5]. Functionalised mesoporous silica has also been electrogenerated at the surface of microelectrodes [16,17]. Macroporous gold was formed on a gold microelectrode to combine the high surface area of a macroporous materials with the high mass transport achieved at a microelectrode [18].

Two methods of chemical modification were selected in this study, namely electrochemically assisted self-assembly formation of sol-gel and nanoporous gold electrodeposition. These two methods were chosen as to our knowledge these two modification methods have not been applied to recessed microelectrode array to date. Mesoporous and nanoporous materials have attracted a wide interest in electroanalysis in recent years [19, 20]. Recent studies have shown that electrochemically assisted self-assembly of silica leads to well-organised mesoporous silica framework with pores oriented perpendicular to the electrode surface [21]. Co-condensation of organo-silane with hydrolysed silane forms mesoporous silica bearing functionalities that can be used for the detection of heavy metals (e.g. $Cu^{2+,}$ Ag^{+}, Hg(II)) [16,17,22]. Nanoporous gold electrodes have also been investigated due to the increase of surface area important for catalytic applications [23-25] apart from biosensor applications.

We investigate here the modification of gold microelectrode arrays achieved by electrogeneration of mesoporous silica on 10 μm microband array and nanoporous gold on 10 μm microdisc array. These particular dimensions were selected due to their stability and reproducibility compared to the nano-dimension counterpart [26]. Electrochemical deposition approach is of interest as it selectively modified the area of interest without smearing the passivation tracks or unwanted area. The porous materials are formed by either a galvanostatic or potentiostatic methods. Although both dip-coating and drop-coating techniques are straight-forward and simple, nevertheless the major concerns associated with these techniques are that they are confined to flat surface and lack for selectivity [27]. The modified microelectrode array are then characterised by cyclic voltammetry (CV), electrochemical impedance spectroscopy (EIS) and scanning electron microscopy (SEM).

2. Material and Methods

2.1. Material and reagents

All chemicals used in this study were purchased from Sigma-Aldrich Ireland Ltd. and used as received. All solutions were prepared with high purity water (18.2 MΩ cm^{-1}) obtained from a Purelab Option from ELGA.

2.2. Microelectrode array fabrication

All microfabrication processing was carried out at the Central Fabrication Facility at Tyndall National Institute according to the procedure for published elsewhere [26]. Following fabrication, the on-chip electrochemical cells wafers were diced and no further electrodes packaging were required. The microelectrode array designs selected for further chemical modification were 10 µm microband array (number of electrodes in array, N=17; width, w=10 µm and length, l=500 µm with centre interspacing, d=100 µm) and 10 µm microdisc array (N= 314; radius, r=5 µm and d=100 µm). Prior modification, the electrodes were exposed to oxygen plasma (Harrick Plasma USA) for 3 min (3 cycles of 1 min at 900 mT pressure and high power settings) to clean and activate the surface.

2.3. Modification methods

For the formation of mesoporous silica films, the microelectrode arrays were first immersed in an ethanolic solution of 20 mM of (3-mercaptopropyl)trimethoxysilane (MPTMS) for 20 minutes. This step allowed the spontaneous adsorption of thiol molecules onto the gold surface. The mesoporous silica films were prepared by the electrochemically assisted self-assembly method described elsewhere [21,28]. Briefly, sol was prepared by mixing ethanol and 0.1 M $NaNO_3$ in 1:1 v/v ratio. Silanes (TEOS:MPTMS 9:1 molar ratio) and CTAB were added to the mixture with total silane concentration of 340 mM. The molar ratio CTAB/silanes was maintained at 0.32 to form regular mesoporous structures as reported [28]. The pH of the sol was adjusted to 3 by addition of HCl and the sol was hydrolysed under stirring at room temperature for 2.5 hours prior to use as electrodeposition medium. The sol was prepared on the day of its use for electrode modification. The electrodes were modified in the hydrolysed sol by a galvanostatic method. Two current densities, j, of -0.74 mA cm^{-2} and -7.4 mA cm^{-2} were used to modify the working electrode in three electrode cell with a silver wire acting as pseudo-reference electrode and a Pt mesh as a counter electrode. After film formation, the electrodes were treated overnight at 135°C (to ensure good cross-linking of the silica network). Template removal was achieved using 0.1 M HCl in ethanol, as previously described [22].

Gold nanostructures were electrodeposited from a solution containing 20 mM $KAu(CN)_2$ and 100 mM $KAg(CN)_2$ in a molar ratio of $Au_{0.18}$:$Ag_{0.82}$ in 250 mM Na_2CO_3, pH 13, as a supporting electrolyte, according to a procedure published by Nagle et al. [25]. Au will undergo selective dissolution during anodic corrosion while Ag is dissolved preferentially. The electrochemical set up consisted of a three electrode system with Ag/AgCl and high surface area Pt coated Ti gauze as reference and counter respectively. The potential of the working electrode was controlled by a CHI 660B instrument. Prior to the surface treatment, all solutions were purged with nitrogen for 20 mins, in order to remove the interfering presence of oxygen. Deposition was carried out at room temperature, by applying a constant potential of -1.2 V for 600 seconds that gave a rate of film at growth of 20 nm min^{-1}.

2.4. Electrochemical measurements and SEM imaging

Electrochemical experiments were performed using a PGSTAT 302N from Ecochemie (Metrohm, United Kingdom) or a CHI660B from CHI Instruments (IJ Cambria, Port Burry, Wales). Bare and modified electrodes were characterised by CV and/or by EIS. In these experiments, the reference electrode was Ag|AgCl|1 M KCl and the counter electrode was a Pt wire. Ferrocenemethanol and ferrocene carboxylic acid were used as redox probes. All experiments were run in 0.01 M PBS or in 0.1 M NaCl. All SEM images were captured using Quanta 650 FEG, Oregon USA.

3. Result and Discussion

3.1. Electrochemically assisted self-assembly (EASA) silica film

Sol-gel electrodeposition technique lends itself well in offering tunable and controlled film thickness formation on an electrode surface. The work on electrodeposition of sol-gel films have been initially described by Shacham et al. in 1999 [29] and the scope of study has been extended by Walcarius and co-workers [16,21]. By applying galvanostatic conditions (i.e. controlling the current) and varying the deposition time, thickness of the films can be accurately controlled and problems with overpotential can be eliminated [30]. A more ordered electrodeposited sol-gel structure could be accomplished by surfactant-templated silica film on electrode surface via electrochemically assisted self-assembly (EASA). The general approach of EASA is similar to the two-step of sol-gel preparation procedures involving hydrolysis of the alkoxide at pH 3 followed by condensation of hydrolysed monomer at pH 9. The condensation leads to the formation of a Si-O-Si bond with the elimination of a water or an alcohol molecule. However in EASA, the pH is being increased by inducing negative potential to the electrode surface [29].

In this EASA study, the electrodes were first pre-treated with a self-assembly partial monolayer using MPTMS before transferring the electrodes into the sol containing CTAB/TEOS:MPTMS (90:10) precursors. The formation of SAM of MPTMS on gold has been proven to act as "molecular glue" between the gold electrode surface and sol-gel derived silica films [31, 32]. The mesoporous silica films were formed on the electrode surface by immersion in a pre-hydrolysed precursor (TEOS) and CTAB at pH 3. A cathodic potential is then applied, increasing the pH and generating hydroxyl ions at the electrode/solution interface. This resulted in the precursor's condensation and concomitant growing of a surfactant-templated mesoporous silica film. Besides served as template, CTAB also have long been reported in sol-gel preparation as to prevent fracture in the film formation [33] and to stabilize the microscopic structure of the material upon heat-drying [34].

The initial approach of electrochemically assisted self-assembly (EASA) of sol-gel in this study was first demonstrated on a 1 mm gold disc electrode surface. CTAB and TEOS precursor ratio of 0.32 was employed; as suggested by Goux et al. [30] in order to attain an aggregate-free thin films. Figure 1 shows the comparison of 1 mm disc gold electrode on an unmodified surface with the electrode after electrodeposition of organosilica film. As can be seen, the apparent advantage of EASA deposition is that the sol-gel was being selectively deposited into the desired electroactive working electrode area without smearing the edges or unwanted areas of the insulating part. The successful deposition of the silica film on the electrode surface in this case can be indicated by changes of the electrode surface colour from pale yellow to bright yellow.

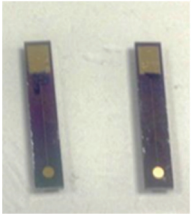


Fig.1. Comparison of colour changes observed at 1 mm gold disc electrode surface on an unmodified electrode (left) and on electrode after sol-gel electrodeposition (right)

The cyclic voltammogram (CV) for the modified electrode was recorded in 5 mM FcMeOH in 0.1 M NaCl with respect to a standard Ag/AgCl reference electrode and Pt wire as counter electrode. The CV after the MPTMS-sol-gel electrodeposition exhibited a shift to a more positive potential indicating the solubility of

the CTAB in FcMeOH (Fig. 2). Upon aging and drying overnight, the sol-gel film seemed to be more repellent as the thiol-functionalised films are hydrophobic hence inducing additional restriction to the mass transport. A better access to the electrode surface was observed after the surfactant template removal which suggests that the template of CTAB surfactant has been successfully removed but the MPTMS with organosilica remained on the gold surface.

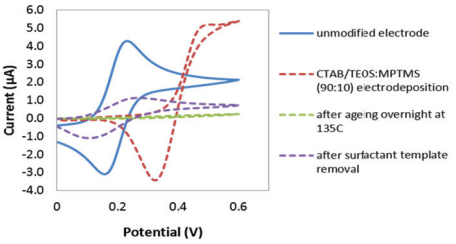


Fig. 2. CVs of the unmodified gold electrode (solid blue line), electrodeposition of CTAB/TEOS:MPTMS precursors on the surface (red dashed line), after aging overnight at 135°C (green dashed line) and after surfactant template removal (purple dashed line). CV recorded in 5 mM FcMeOH in 0.1M NaCl (scan rate 50 mV s^{-1}). Potential achieved after deposition time of 8 secs was -1.3 V

3.1.1. EASA silica film on recessed microband array

The EASA deposition method had been successfully applied to electrodes with various morphology, geometry and size, namely macroelectrode, microwire, microdisc and Au-CD-trode [16]. However the electrodeposition of silica film on recessed microband array has not been assessed to date. It was observed that applying the same current density of -0.74 mA cm^{-2} as on the 1 mm gold disc electrode on microelectrode array did not lead to the sol-gel electrodeposition despite extending the deposition time. When moving from macro- to smaller electrode dimensions, larger current densities need to be applied in ensuring the film deposition. This is attributed to the faster loss of the hydroxyl species in the solution for the diffusion profile of radial or spherical in microelectrode in comparison with linear diffusion on planar macroelectrode [16].

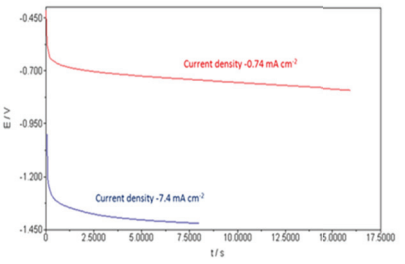


Fig. 3. Potential as a function of time for the different current density applied for 10 μm microband array. Lower potential achieved for the sol-gel silica film electrodeposition once the current density was increased despite the deposition time. The current density hence needs to be increased when moving from a macro electrode.

Effects of ageing temperature on silica film's size

The silica film formed on the recessed microband array aged at 135^{o}C overnight was found to consist of big granulars (Fig. 4). The formation of such big granules could be attributed to several factors. Firstly, it was postulated that current density applied being so high that the film was formed inside the recess before reaching the surface of the silicon nitride thus depositing outside the recess. Interestingly, the cylindrical diffusion process that is commonly associated with microband array could be directly observed in the SEM image. This could be seen on the cylindrical silica-film formed on the recess. Secondly, the silica film also could be densified during the ageing process where the electrode was placed in an oven with temperature of 135°C. It is proposed that, during gel densification, the desiccated gel become more highly cross-linked while reducing its surface area and free volume [35]. While this effect is not prominent on larger surface, a much smaller surface is greatly affected with the high temperature [36] where densification temperature decreases as the pore radius decreases and surface area of the gels increases. Although Herzog et al. (2013) did not encounter this densification when modifying the microelectrodes [16], it is noteworthy to mention that the recessed microelectrodes used in this study had different geometry.

The microband electrode was then left ageing overnight at room temperature instead of high temperature in the oven. Smoother silica film with spheres ranging from 300-500 nm was successfully deposited on gold microband array within the recess trench. The permeability properties and electrochemical properties of the films aged at the room temperature is discussed in the next section.

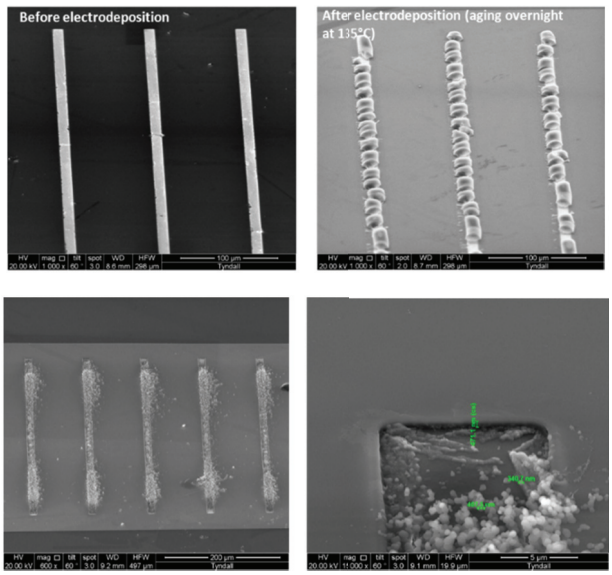


Fig. 4. *Top row:* SEM images of unmodified microband array (right) and after CTAB/TEOS:MPTMS (90:10) electrodeposition aged overnight at 135^{o}C. *Bottom row*: SEM images of silica beads successfully deposited on recessed gold microband array (left) with closed up image (right) when left ageing overnight at room temperature.

3.1.2. Electrochemical characterisations for sol-gel modified microelectrode array

The thin film of small silica beads formed within the microbands' recess trench is indicated by a low and compressed CV signal which correlates to the blocking of electron transfer on the electrode surface. However, after surfactant template removal in ethanolic solution, a better permeability of the film was observed. Interestingly, the modified microband with silica film still retained its microelectrode behaviour.

This suggests that the whole band surfaces has opened up several template spots that may be in resemblance with disc hence a steady-shaped voltammogram was observed.

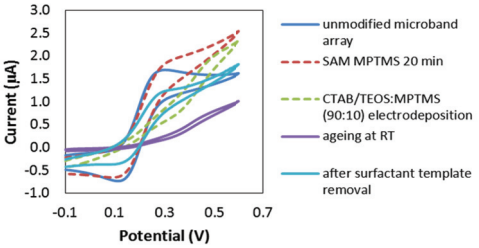


Fig. 5. CVs of the unmodified microband array (solid dark blue line), after self-assembly MPTMS for 20 minutes (red dashed line), electrodeposition of CTAB/TEOS:MPTMS precursors on the surface (green dashed line), after aging overnight at room temperature (purple solid line) and after surfactant removal (light blue line). CV recorded in 5 mM FcMeOH in 0.1M NaCl (scan rate 50 mV s^{-1}). Potential achieved after deposition time of 8 secs was -1.14 V, current density -7.4 mA cm^{-2}.

The EIS study was also carried out to assess the microelectrode behaviour upon modifications. Following the partial self-assembly of MPTMS, a shift on the impedance took place (inset, top diagram). A significant increment of the impedance was seen straight after the sol-gel and MPTMS electrodeposition. A massive blocking behaviour was observed after an overnight aging confirming the hardening of the silica film that blocked the electron from reaching the surface. Better permeability occured on the electrode once the surfactant template removal was performed. These results are in agreement with the results obtained by cyclic voltammetry analysis. While the advantage of microelectrode was maintained after the surfactant removal (steady state CV), EIS study has confirmed the change of the diffusion profile on the modified surface. The impedance is now tending to straight line indicating planar diffusion on the modified electrode. Such behaviour could be attributed to the greater diffusivity of the redox solution within the silica film [37]. Similar pattern has been reported also by Wei & Hillhouse (2007) for their modified cubic silica films in ferrocene dimethanol redox solution [38].

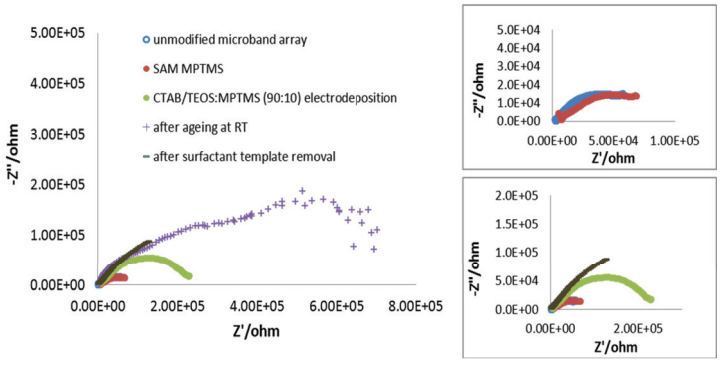


Fig. 6. EIS of the unmodified microband array (inset, top diagram- blue marker), after self-assembly MPTMS for 20 minutes (inset, top diagram- red marker), electrodeposition of CTAB/TEOS:MPTMS precursors on the surface (green marker), after aging overnight at room temperature (purple marker) and after surfactant template removal (grey marker). EIS recorded in 5 mM FcMeOH in 0.1M NaCl (0.1-1 MHz).

3.2. Nanoporous gold modified surface for microdisc array

3.1.1. SEM analysis

The objective of modifying the electrode area with nanoporous gold (NPG) is to increase the active surface area of the gold electrode. The sensitivity of biosensor has been proven to be improved by making the surface porous compared to a planar gold surface [39,40]. The porosity allows a larger number of biomolecules attachments per surface area resulting in larger signal upon binding with their specifically binding analyte molecules. SEM images in Fig. 7 show modified 10 μm microdisc electrode array with NPG of different thickness. The thickness of the NPG is controlled by the time of electrodeposition. Prior to the modification, two of the microdiscs have recess depths of 917 nm and one with 735 nm. After the modification, NPG of three different thicknesses has been successfully deposited (122 nm, 252 nm and 6.8 μm). From the images, it can be seen that NPG appears as sponge-like 3D structure with interconnecting pores with ligaments (Fig. 7d). Despite its porous structure, it has been shown that NPG can be as strong as bulk Au [41,42].

3.1.2. Electrochemical characterisations for NPG-modified microelectrode array

CVs were recorded in 1 mM ferrocene carboxylic acid (FCA) in PBS (pH 7.4) with respect to a standard Ag/AgCl reference electrode and Pt wire as the counter electrode. The limiting current for the recess depth thickness after modification was calculated and compared to the obtained experimental limiting current. The following equations describe the limiting current for both recessed microelectrode array and hemisphere electrode [43].

For recessed microdisc array,

$$i_{lim} = \left(\frac{4\pi nFCDr^2}{4L + \pi r}\right)N \quad (1)$$

And for hemisphere electrode,

$$i_{lim} = (2\pi nFDCr)N \quad (2)$$

where where n is the number of electrons involved in the reaction, F is Faraday constant (96,485 C mol^{-1}), C is the bulk concentration of ferrocene carboxylic acid (mol cm^{-3}), D is diffusion coefficient (5.7×10^{-6} cm^2 s^{-1}), r is the disc radius (cm), L is the silicon nitride thickness (recess depth) (cm) and N is the number of the disc electrodes in an array.

The modified NPG microelectrode exhibits highly improved electrochemical responses compared to the readily fabricated microelectrode, owing to its high surface area. As can be seen from Table 1, the experimental limiting currents obtained are twice as large as the theoretical limiting current. This has arisen from the mass transport of the redox solution occurring through porosity of the NPG across the electrode surface.

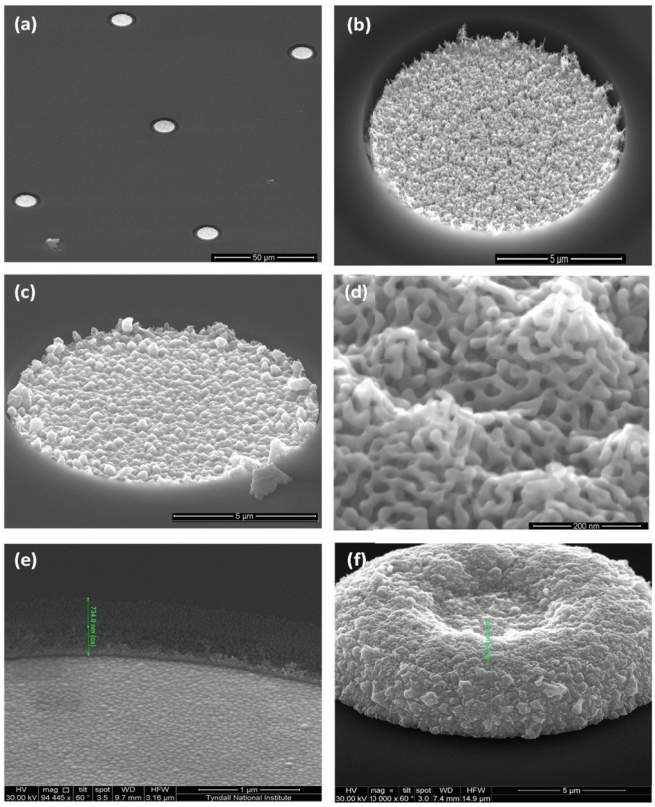


Fig. 7. SEM images of NPG-modified 10 µm microdisc array with 917 nm recess depth (a-d): (a) microdisc array after modification; (b) 122 nm NPG deposited; (c) 252 nm NPG deposited; (d) close-up image of NPG with the joint ligament; and modified microdisc with 735 nm recess depth (e-f): (e) disc before modification; (f) NPG with 6.8 µm NPG deposition. Images are tilted to 60°.

Table 1 Comparison between theoretical current and experimental current for NPG-modified microelectrodes

	Theoretical current (nA)	**Experimental current (nA)**
Initial microdisc recess of 917 nm		
795 nm recess (after 122 nm NPG deposited)	287	564.94 ± 44.49
665 nm recess depth (after 252 nm NPG deposited)	295	627.01 ±97.08
Initial microdisc recess of 735 nm		
Hemisphere electrode of 6.1 µm (after NPG deposition of 6.8 µm)	543	1160 ± 498.97

From the NPG-modified microelectrodes with recess depth of 795 nm and 665 nm, it was found that the current density with regard to the calculated theoretical current has increased from 1.16 mA cm^{-2} to 2.29 mA cm^{-2} and from 1.2 mA cm-2 to 2.54 mA cm^{-2} respectively. In both cases, a current density increment of twice was observed. Interestingly, the current density obtained is in the same vicinity as reported by Nagle & Rohan (2011) for NPG-modified planar Au electrode (3.1 mA cm^{-2}). The value for the current density at the unmodified planar Au with 5 mm diameter macro disc was 2.65 mA cm^{-2} [44]; which indicate

the modified NPG-recessed microdisc array has a current density that is on par with the macrodisc area. For the NPG-modified microdisc electrode with 6.1 μm hemisphere formed above the recess, a current density increment of twice was also observed (from 2.2 mA cm^{-2} to 4.7 mA cm^{-2}).

It was found that the characteristic of microelectrode of having a steady-state CV has diminished for the NPG-modified microelectrode with hemisphere NPG formed above the recess. A broad and peak-shaped CV that corresponds to a macroelectrode CV was attained at scan rate at 100 mV s^{-1} (Fig. 8). The respective EIS also has the lowest values in comparison with the unmodified and other NPG-modified microdisc electrodes (Fig. 9). This is due to the protruding geometry of the formed NPG-hemisphere that permits easier electron transfer at the surface and hence lower impedance.

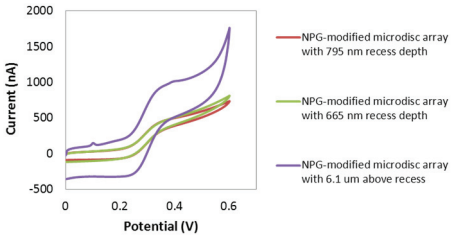


Fig. 8. CV of the NPG-modified microdisc array of different thicknesses. Scan rate 100 mV s^{-1} in 1 mM FCA in PBS pH7.4.

The two other NPG-modified microdiscs on the other hand, exhibited steady-shaped voltammograms at 100 mV s^{-1}. Supposedly the EIS of the NPG-modified microdisc with 795 nm recess depth exhibited higher impedance compared to the of 695 nm recess depth. In this case, for the 665 nm recess depth, 225 nm of NPG was formed hence the film is thicker compared to the 122 nm of NPG formed that resulted in 795 nm recess depth. However no significant difference was observed between the two. This can be addressed to the SEM images as only one disc from the disc array of 314 electrodes was taken. The NPG thickness could be vary from one disc to another disc, and the EIS shows the impedance of total surface area instead of one disc alone. The striking importance however is that a 25-fold decrease in impedance of NPG-modified electrode was reported compared to unmodified gold electrode, as a result of the augmented total surface area [45].

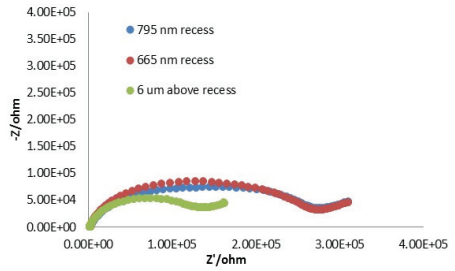


Fig. 9. EIS of the NPG-modified microdisc array of different thicknesses in 1 mM FCA in PBS. Frequency applied was 0.01-1 MHz.

These interesting features of the NPG-modified microdisc in terms of electrochemistry and surface roughness provide a promising feature for its future application in biosensor area. The modified microdisc array electrode has been applied in dissolved oxygen sensing application which will be used for monitoring of drinking water quality in rural communities in India [46].

4. Conclusion

For the sol-gel silica film formation, MPTMS pre-treatment exhibited successful formation of the sol-gel on the gold electrode surface. Silica film deposition is possible on recessed microband array but the characteristics for film formation greatly dependent on the experimental conditions i.e. increasing the current density when moving from macro to micro dimension. Ageing the microelectrode at high temperature leads to the poor formation of the silica gels. We also have demonstrated that NPG-modified recessed microdisc can be conveniently prepared by dealloying steps. This direct and simple method provides a rougher surface with higher current density while maintaining the merit of microelectrode behaviour. The microdisc array still retains its microelectrode behaviour (in the case of presence recessed NPG layer). The integration of surface roughness increment and microelectrode properties may help in improving the biosensing application. The film thickness formed via EASA and NPG for modifying gold electrode surface could be tuned by controlling the electrodeposition parameters (time and ratio of mixtures) thus offering wide range of further biosensor applications.

Acknowledgements

We would like to thank Mr. Vince Lodge from Central Fabrication Lab, Tyndall National Institute for the SEM images. Special gratitude for Malaysian Agricultural Research & Development Institute (MARDI) for the scholarship.

References

1. Wightman RM, David OW. Voltammetry at ultramicroelectrodes. *Electroanalytical chemistry* 1989; **15**:267-353.
2. Kovacs GTA. *Micromachined transducers sourcebook*. New York: WCB/McGraw-Hill; 1998.
3. Moujahid W, Eichelmann-Daly P, Strutwolf J, Ogurtsov VI, Herzog G, Arrigan DW. Microelectrochemical systems on silicon chips for the detection of pollutants in seawater. *Electroanalysis* 2011; **23**:147-155.
4. Suzuki H. Microfabrication of chemical sensors and biosensors for environmental monitoring. *Materials Science and Engineering: C* 2000;**12**:55-61.
5. Parker CO, Lanyon YH, Manning M, Arrigan DW, Tothill IE. Electrochemical immunochip sensor for aflatoxin M1 detection. *Analytical Chemistry* 2009;**81**:5291-5298.
6. Lauks IR. Microfabricated biosensors and microanalytical systems for blood analysis. *Accounts of Chemical Research*, 1998;**31**: 317-324.
7. Huang XJ, O'Mahony AM, Compton RG. Microelectrode arrays for electrochemistry: Approaches to fabrication. *Small* 2009; **5**:776-788.
8. Torres-Rodriguez LM, Roget A, Billon M, Bidan G, Livache T. Synthesis of a biotin functionalized pyrrole and its electropolymerization: toward a versatile avidin biosensor. *Chemical Communications* 1998;**18**:1993-1994.
9. Pritchard J, Law K, Vakurov A, Millner P, Higson SP. Sonochemically fabricated enzyme microelectrode arrays for the environmental monitoring of pesticides. *Biosensors and Bioelectronics* 2004;**20**:765-772.
10. Gómez-Caballero A, Unceta N, Goicolea MA, Barrio RJ. Voltammetric determination of metamitron with an electrogenerated molecularly imprinted polymer microsensor. *Electroanalysis* 2007;**19**:356-363.
11. Gómez-Caballero A, Goicolea MA, Barrio RJ. Paracetamol voltammetric microsensors based on electrocopolymerized–molecularly imprinted film modified carbon fiber microelectrodes. *Analyst* 2005;**130**:1012-1018.
12. Cooper JS, Raguse B, Chow E, Hubble L, Müller KH, Wieczorek L. Gold nanoparticle chemiresistor sensor array that differentiates between hydrocarbon fuels dissolved in artificial seawater. *Analytical chemistry* 2010; **82**:3788-3795.

13. Chow E, Gengenbach, TR, Wieczorek L, Raguse B. Detection of organics in aqueous solution using gold nanoparticles modified with mixed monolayers of 1-hexanethiol and 4-mercaptophenol. *Sensors and Actuators B: Chemical* 2010;**143**:704-711.
14. Chen Y, Pui TS, Kongsuphol P, Tang KC, Arya SK. Aptamer-based array electrodes for quantitative interferon-γ detection. *Biosensors and Bioelectronics* 2014;**53**:257-262.
15. Tolba M, Ahmed MU, Tlili C, Eichenseher F, Loessner MJ, Zourob, M. A bacteriophage endolysin-based electrochemical impedance biosensor for the rapid detection of Listeria cells. *Analyst* 2012;**137**:5749-5756.
16. Herzog G, Sibottier E, Etienne M, Walcarius, A. Electrochemically assisted self-assembly of ordered and functionalized mesoporous silica films: impact of the electrode geometry and size on film formation and properties. *Faraday discussions*, 2013;**164**:259-273.
17. Herzog G, Vodolazkaya NA, Walcarius A. Platinum ultramicroelectrodes modified with electrogenerated surfactant-templated mesoporous organosilica films: effect of film formation conditions on its performance in preconcentration electroanalysis. *Electroanalysis* 2013;**25**:2595-2603.
18. Szamocki R, Velichko A, Holzapfel C, Mücklich F, Ravaine S, Garrigue P et al. Macroporous ultramicroelectrodes for improved electroanalytical measurements. *Analytical chemistry* 2007;**79**:533-539.
19. Walcarius A. Mesoporous materials and electrochemistry. *Chemical Society Reviews* 2013;**42**:4098-4140.
20. Hou X, Guo W, Jiang L. Biomimetic smart nanopores and nanochannels. *Chemical Society Reviews* 2011;**40**:2385-2401.
21. Walcarius A, Sibottier E, Etienne M, Ghanbaja J. Electrochemically assisted self-assembly of mesoporous silica thin films. *Nature materials* 2007;**6**:602-608.
22. Etienne M, Goux A, Sibottier E, Walcarius, A. Oriented mesoporous organosilica films on electrode: a new class of nanomaterials for sensing. *Journal of nanoscience and nanotechnology* 2009;**9**: 2398-2406.
23. Scanlon MD, Salaj-Kosla U, Belochapkine S, MacAodha D, Leech D, Ding Y et al. Characterization of nanoporous gold electrodes for bioelectrochemical applications. *Langmuir* 2012;**28**:2251-2261.
24. Jiang J, Wang X. Fabrication of high-surface nanoporous gold microelectrode. *Electrochemistry Communications* 2012;**20**:157-159.
25. Nagle LC, Rohan JF. Nanoporous gold anode catalyst for direct borohydride fuel cell. *international journal of hydrogen energy* 2011;**36**:10319-10326.
26. Said NAM, Twomey K, Ogurtsov VI, Arrigan DW, Herzog G. Fabrication and electrochemical characterization of micro-and nanoelectrode arrays for sensor applications. *Journal of Physics: Conference Series* 2011; **307**: 012052
27. Walcarius A, Mandler D, Cox JA, Collinson M, Lev O. Exciting new directions in the intersection of functionalized sol–gel materials with electrochemistry. *Journal of Materials Chemistry* 2005;**15**:3663-3689.
28. Goux A, Ghanbaja J, Walcarius A. Prussian Blue electrodeposition within an oriented mesoporous silica film: preliminary observations. *Journal of materials science* 2009;**44**:6601-6607.
29. Shacham R, Avnir D, Mandler D. (1999). Electrodeposition of methylated sol-gel films on conducting surfaces. *Advanced Materials* 1999;**11**: 384-388.
30. Goux A, Etienne M, Aubert E, Lecomte C, Ghanbaja J, Walcarius, A. Oriented mesoporous silica films obtained by electro-assisted self-assembly (EASA). *Chemistry of Materials* 2009;**21**:731-741.
31. Sibottier E, Sayen S, Gaboriaud F, Walcarius A. (2006). Factors affecting the preparation and properties of electrodeposited silica thin films functionalized with amine or thiol groups. *Langmuir* 2006;**22**:8366-8373.
32. Wang J, Pamidi PV, Zanette DR. *Self-assembled silica gel networks.* Journal of the American Chemical Society 1998;**120**(23): 5852-5853.
33. Li J, Tan SN, Ge H. *Silica sol-gel immobilized amperometric biosensor for hydrogen peroxide.* Analytica Chimica Acta 1996; **335**:137-145.
34. Rottman C, Grader G, De Hazan Y, Melchior S, Avnir, D. Surfactant-induced modification of dopants reactivity in sol-gel matrixes. *Journal of the American Chemical Society* 1999;121:8533-8543.
35. Brinker CJ, Scherer GW., *Sol → gel → glass: I. Gelation and gel structure.* Journal of Non-Crystalline Solids 1985; **70**:301-322.
36. Hench LL, West JK. *The sol-gel process.* Chemical Reviews 1990;**90**:33-72.

37. Etienne M, Guillemin Y, Grosso D, Walcarius A. Electrochemical approaches for the fabrication and/or characterization of pure and hybrid templated mesoporous oxide thin films: a review. *Analytical and bioanalytical chemistry* 2013;**405:**1497-1512.
38. Wei T-C, Hillhouse HW. *Mass transport and electrode accessibility through periodic self-assembled nanoporous silica thin films.* Langmuir 2007;**23**:5689-5699.
39. van Noort D, Mandenius C-F. *Porous gold surfaces for biosensor applications.* Biosensors and Bioelectronics 2000;**15**:203-209.
40. Hu K, Lan D, Li X, Zhang S. Electrochemical DNA biosensor based on nanoporous gold electrode and multifunctional encoded DNA− Au bio bar codes. *Analytical chemistry* 2008;**80**:9124-9130.
41. Erlebacher J, Aziz MJ, Karma A, Dimitrov N, Sieradzki K. Evolution of nanoporosity in dealloying. *Nature* 2001;**410:**450-453.
42. Biener J, Hodge AM, Hayes JR, Volkert CA, Zepeda-Ruiz LA, Hamza AV et al. Size effects on the mechanical behavior of nanoporous Au. *Nano letters* 2006;**6**:2379-2382.
43. Arrigan DW. *Nanoelectrodes, nanoelectrode arrays and their applications.* Analyst 2004;**129**:1157-1165.
44. Nagle LC, Rohan JF. *Nanoporous gold catalyst for direct ammonia borane fuel cells.* Journal of the Electrochemical Society, 2011;**158**:B772-B778.
45. Seker E, Berdichevsky Y, Begley MR, Reed ML, Staley KJ, Yarmush ML. The fabrication of low-impedance nanoporous gold multiple-electrode arrays for neural electrophysiology studies. *Nanotechnology* 2010;**21**:125504.
46. Twomey K, Nagle LC, Said A, Barry F, Ogurtsov VI. Characterisation of nanoporous gold for use in a dissolved oxygen sensing application. *BioNanoScience* 2015;**5**:55-63.